Applied Catalysis A: General 485 (2014) 222–229

Contents lists available at ScienceDirect

Applied Catalysis A: General

journal homepage: www.elsevier.com/locate/apcata

Oxide layers with Pd-containing nanoparticles on titanium

I.V. Lukiyanchuk[a,*], E.K. Papynov[a], V.S. Rudnev[a,b], V.A. Avramenko[a,b], I.V. Chernykh[a], L.M. Tyrina[a], A.Yu. Ustinov[a,b], V.G. Kuryavyi[a,b], D.V. Marinin[a]

[a] Institute of Chemistry, Far-Eastern Branch, Russian Academy of Sciences, Vladivostok, Russia
[b] Far-Eastern Federal University, Vladivostok, Russia

ARTICLE INFO

Article history:
Received 18 April 2014
Received in revised form 24 July 2014
Accepted 6 August 2014
Available online 15 August 2014

Keywords:
Titanium
Plasma electrolytic oxidation
Template sol–gel synthesis
Multicomponent oxide coatings
Palladium nanoparticles
CO oxidation

ABSTRACT

$PdO_x/SiO_2 + TiO_2/Ti$ composites with different palladium contents have been fabricated by a combination of plasma electrolytic oxidation and template sol–gel synthesis on titanium substrates. The effect of multiplicity of deposition of titanium hydroxide gel with palladium nanoparticles on the composite composition and the surface morphology has been investigated. It has been established that the coatings surface is heterogeneous: it is built from alternating sites of different types with varying palladium content. Palladium is concentrated in nanosized structures of a diameter of 25–60 nm. The fabricated composites catalyze the reaction of oxidation of CO into CO_2 at temperatures above 170 °C. It has been demonstrated that at the average concentration of palladium in coatings equal to 0.04 at.% the activation energy for this reaction is equal to ~55 kJ/mol, whereas at 0.1–0.2 at.% it is equal to ~46 kJ/mol.

1. Introduction

Catalysts based on platinum group metals (Pt, Pd, Rh) deposited on ceramic and metal parts find extensive application in afterburning of exhaust gases of internal combustion engines [1–6], deep oxidation of CO and hydrocarbons [7–11], and a number of other oxidation–reduction reactions [12–14].

The use of noble metals in the form of nanoparticles (1–50 nm in size) dispersed on oxide supports has been received much attention [15–20]. On the one hand, it reduces the noble metal consumption; on the other hand, it allows fabrication of catalysts having high activity in low-temperature CO oxidation [9,11,21,22]. For example, the catalysts with Au nanoparticles with diameters below 5 nm are active in CO oxidation at room temperatures [18,23,24].

To deposit noble metals as nanoparticles on oxide support, different methods are used [25,26]: gas–thermal sputtering [27,28], deposition from solutions [18,23,29], sol–gel synthesis with use of templates [30–35] etc. Each method has its advantages and disadvantages in terms of adhesion, attachment, particle dispersion and size, and catalysts' mechanical properties. A support for catalytically active substances application has an important role in proving mechanical, physical, and thermal properties of these catalysts. The supports in the form of the oxide layer of a small thickness, which are deposited on metallic substrates, can give heat conductivity, electrical conductivity and mechanical stability to the catalysts [6]. Such catalysts on metal substrates are promising for use in constructions of microreactors for coupled reactions and environmental catalysis [36–41].

The supports "oxide layer/metal" can be fabricated by the plasma electrolytic oxidation (PEO) technique [36,37,42–51]. This technique consists in electrochemical oxidation of valve metals under spark and microarc electrical discharge conditions [52–55]. Using this method and its combinations with impregnation or extraction pyrolysis, catalytically active coatings containing noble metals [36,42–44] and compounds of transition metal [36,37,46–51] were fabricated.

Up to present, we do not know the works on the use of the combination of plasma electrolytic oxidation and template sol–gel synthesis to produce catalysts on metal substrates. *The objective* of the present work was to study the composition and structures of Pd-containing catalysts on titanium substrates fabricated by a combination of the methods of plasma electrolytic oxidation and template sol–gel synthesis and estimate their activity in CO oxidation.

2. Experimental

2.1. PEO coatings fabrication

PEO-coatings were fabricated on samples of titanium of the grade VT1-0 (99.9% Ti). Samples of two types were used: flat samples of a size of 0.7 × 1.4 × 0.1 cm and those twisted into wire spirals

* Corresponding author. Tel.: +7 (423) 2215265; fax: +7 (423) 2312590.
E-mail address: lukiyanchuk@ich.dvo.ru (I.V. Lukiyanchuk).

http://dx.doi.org/10.1016/j.apcata.2014.08.007
0926-860X/

of the crosscut diameter of 1.2 mm with the geometric surface area of 20 cm^2. The former samples were used for subsequent determination of the element and phase composition of the deposited coatings; the latter ones were used in catalytic tests of the obtained coating/metal composites.

For the sake of surface standardization, titanium samples were polished in a mixture of hydrofluoric and nitric acids HF:HNO_3 = 1:3 at 70 °C for 2–3 s prior to anodization [56]. Upon chemical polishing, samples were washed (first, by tap water, then by distilled water) and dried in air at 70 °C.

PEO-coatings were formed in an aqueous solution of 0.05 mol/L Na_2SiO_3 + 0.05 mol/L NaOH. The electrolyte was prepared on the basis of distilled water and commercially available reagents: $Na_2SiO_3 \cdot 9H_2O$ of the analytical pure grade and NaOH of the chemical pure grade (III). The choice of the silicate alkali electrolyte is caused by the possibility of formation of coatings with developed surface and high humidity absorption [51].

Oxide layers were formed in the galvanostatic mode at anodic polarization of samples (current density i = 10 A/dm^2, treatment time t = 10 min). A PC-controlled commercial TER-4/460N thyristor unit (Russia) was used as a current source. The synchronizer unit and software were developed by JSC Fleron (Vladivostok, Russia). The electrochemical cell used in anodization consisted of a glass of a volume of 1 L and a cathode in the form of a coil pipe: a hollow tube made of the corrosion-resistant steel of the grade 12Kh18N10T. Cold tap water was passed through the coil pipe for cooling. The solution was stirred using a magnetic stirrer. The solution temperature during the process did not exceed 50 °C.

2.2. Deposition of Pd-containing layers by template sol–gel synthesis

Pd-containing composites were formed by dipping oxidized titanium samples into sol containing hydrated titanium dioxide with palladium nanoparticles immobilized inside micelles of siloxane-acrylate emulsion followed by drying and annealing. The sol preparation method is similar to that described in refs. [30,31].

A commercial aqueous siloxane-acrylate emulsion KE 13-36 (JSC Astrokhim, Elektrostal', Russia) with the solid phase content of 50% and the average micelle size of 160 nm was used as a template. The structure of emulsion is analogous to that of shell copolymer shown in ref. [57]. Emulsion functionalization was carried out by addition of the required amount of H_2PdCl_4 and subsequent heating at 100 °C for 30 min. The chloropalladic (II) acid solution was prepared by dissolution of the metallic palladium in aqua regia followed by evaporation:

$$3Pd + 4HNO_3 + 18HCl \rightarrow 3H_2[PdCl_6] + 4NO\uparrow + 8H_2O.$$

$$3H_2[PdCl_6] \rightarrow H_2[PdCl_4] + Cl_2\uparrow .$$

Functionalization resulted in palladium ions embedding into the emulsion structure. The functionalized emulsion solution was added with 16% hydrochloric acid solution of $TiCl_3$ (strong reducer), which hydrolysis yielded a stable sol of titanium hydroxide containing palladium nanoparticles in the emulsion micelle composition. In other words, the process of titanium hydroxide sol formation was accompanied by palladium reduction until the metal state. The palladium concentration in such a sol was about 0.08 mg/mL or 7.5×10^{-3} mol/L.

Samples with PEO-coatings were dipped into sol for 1 s with intermediate drying in air at 90 °C. In such a way, samples undergoing 5-, 10-, 15-, and 20-fold dipping-drying cycles with final annealing of each series in air at 500 °C were obtained. At this temperature, palladium is oxidized to PdO. Hereinafter, these samples are marked as **5Pd**, **10Pd**, **15Pd**, and **20Pd** in the text. The number of dipping-drying cycles or operations is marked as *N*.

The scheme of the metal/coating composite formation by combination of PEO and sol–gel synthesis and the suggested structure of the composite are shown in Fig. 1.

2.3. Coatings characterization

The data on the samples morphology and element composition were obtained using a Hitachi S5500 high-resolution scanning electron microscope (Japan) equipped with a Thermo Scientific accessory for energy-dispersive analysis (USA). Gold was preliminarily sputtered on samples to prevent surface charging. The depth of scanning beam penetration was ~1 μm. The average composite element composition at scanning was at least five sites of a size of 100 × 100 μm.

X-ray images were recorded on a Bruker D8 ADVANCE X-ray diffractometer (Germany) in Cu K_α-radiation. During the X-ray diffraction analysis (XRD), the search program EVA with the database PDF-2 was used.

For the surface composition analysis, the method of X-ray photoelectron spectroscopy (XPS) was used. The XPS spectra were measured on samples of a size of 0.7 × 1.3 cm at a depth of ~3 nm using a Specs high-vacuum device (Germany) with a 150-mm electrostatic analyzer. A part of the sample surface of a diameter of ~5 mm was analyzed. Mg K_α radiation was applied for ionization. The working vacuum was 2×10^{-7} Pa. The spectra calibration was carried out on C1s-lines of hydrocarbons, whose energy was stated to be equal to 285.0 eV. Etching by high-energy argon ion beam was used to remove the surface layer of a thickness of ~3 nm.

2.4. Catalytic tests

Catalytic tests were carried out on a BI-CATr-EXP flow-circulation catalytic device (JSC Advanced Laboratory Equipment, Novosibirsk, Russia) for the reaction of oxidation of CO into CO_2. The device is used to determine the catalytic activity (stationary specific rate of the reaction W, mL/g s) at fixed parameters: preset reaction temperature (T, K) and composition of the contact reaction mixture contacting with the catalyst surface. Titanium wire with deposited Pd-containing coatings (the sample weight was about 2.5 g, the geometric area of the coating surface was 20 cm^2) was cut into a few parts and placed inside a cylindrical removable holder of a tubular metallic reactor (reactor volume 20 mL, diameter 30 mm). A scheme of the reactor and the image of the coated sample from titanium wire are shown in the Fig. 2.

The initial reaction mixture contained 1% CO and air. The CO concentration in the composition of initial and final reaction mixtures was determined using a built-in chromatograph equipped with a thermal-catalytic detector. The studied temperature range was 20–500 °C. For any specific temperature T, the reaction rate W_{50} at 50% conversion of CO into CO_2 (X = 50%) was found. The gas flow rate was controlled from 50 up to 1200 mL/min. The activation energy E_a was estimated on the basis of dependencies of the reaction rate logarithm W_{50} for 50% conversion of CO on the inverse temperature.

3. Results

In the course of plasma electrolytic oxidation of titanium, composites of the type 'PEO-coating/Ti' are formed. According to the XRD analysis data, only titanium oxides in anatase and rutile modifications were found in the composition of coatings formed in the silicate electrolyte, whereas silicon dioxide was not found. Taking into account the fact that, according to the energy-dispersive analysis data, coatings contain substantial amounts of silicon (at.%: 21.1

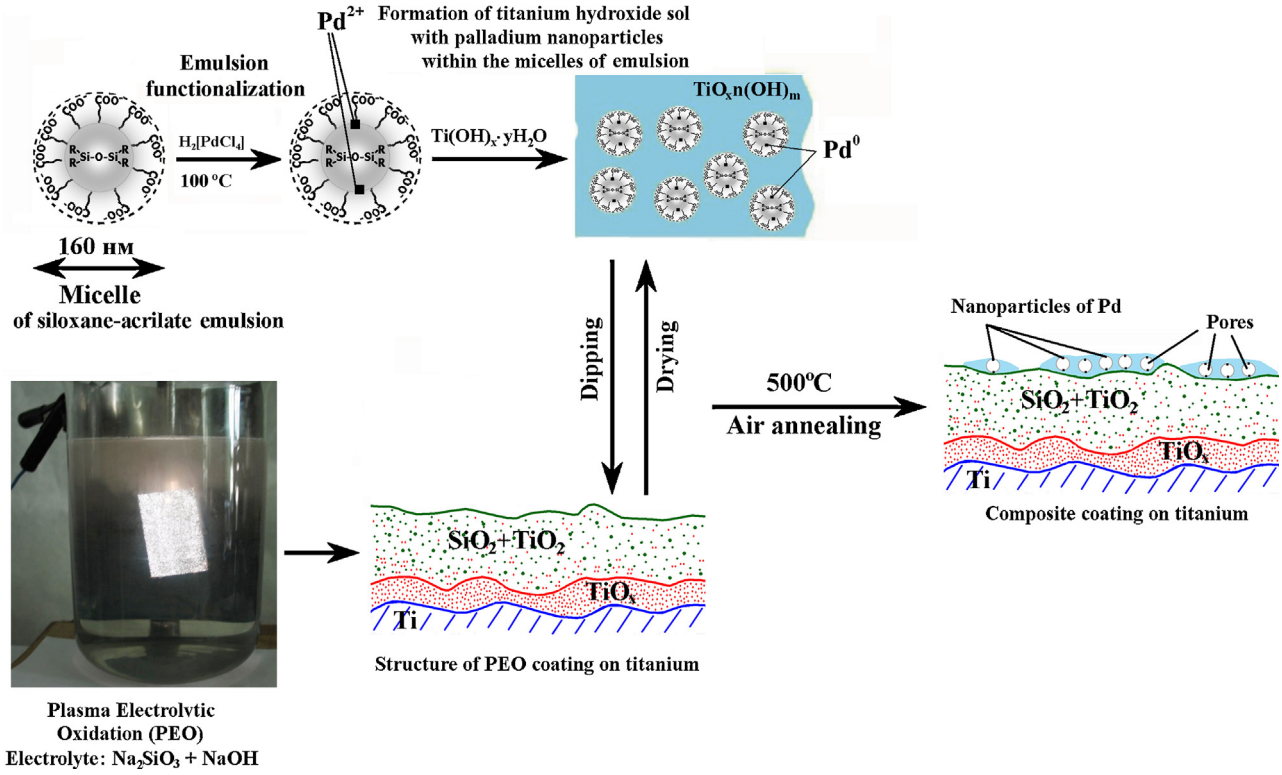

Fig. 1. Scheme of coatings fabrication by combination of plasma electrolytic oxidation in silicate electrolyte and sol–gel synthesis with application of siloxane-acrylate emulsion with immobilized palladium particles as a template.

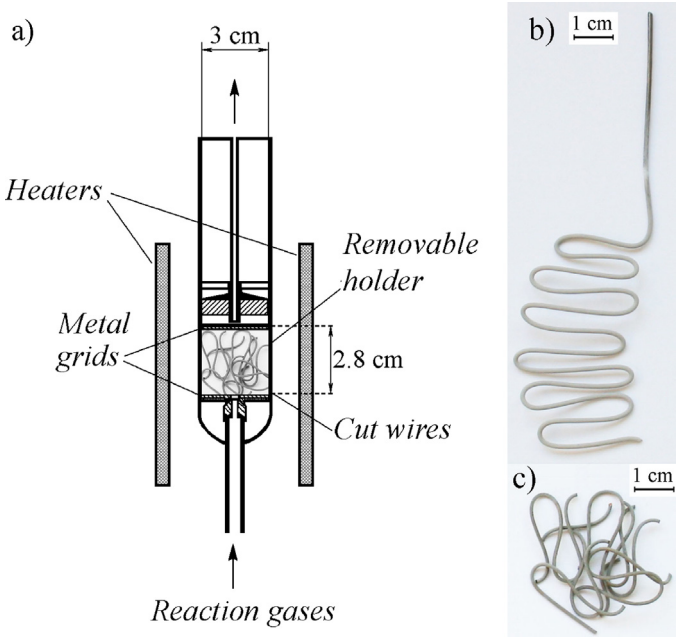

Fig. 2. A scheme of the reactor (a) and the images of samples from titanium wire with Pd-containing coating before (b) and after cutting (c).

Si, 9.2 Ti, 0.9 Na, 59.8 O, 9.1 C), one can assume that it is present in the composition of amorphous silica, and, therefore, the composites can be represented as $SiO_2 + TiO_2/Ti$. Note that the PEO-coating thickness is 9 ± 2 μm.

As was shown by the XPS data, upon the operations of sol deposition, drying, and annealing, the coatings contained titanium, oxygen, silicon, carbon, sodium, palladium, and nitrogen (Table 1, Fig. 3). The presence of the latter must be the result of interaction of the atmospheric nitrogen with the coating surface. The surface and subsurface layers of the composites under study (5Pd, 10Pd, 20Pd) are virtually identical with respect to qualitative and quantitative composition. In the subsurface layer, titanium is present predominantly as TiO_2 (binding energy E_b = 459.0 eV, table value of E_b for TiO_2 – 458.7 eV). Upon etching, TiO is also present in addition to TiO_2 (peak broadening takes place). In the surface layer, silicon is present as SiO_2 (E_b = 103.1 eV, table value of E_b for SiO_2 – 103.0 eV). The average palladium concentration on the surface is 0.1–0.3 at.%. According to binding energy values, Pd^{2+} ($E_b(Pd3d_{5/2})$ = 337.0 eV) is present along with Pd^0 ($E_b(Pd3d_{5/2})$ = 335.0 eV). Upon etching with argon, just oxidized palladium was found. In this case, the value $E_b(Pd3d_{5/2})$ = 336.0–336.4 eV is intermediate between the binding energies of metallic palladium ($E_b(Pd3d_{5/2})$ = 335.0 eV) and PdO ($E_b(Pd3d_{5/2})$ = 337.0 eV). In the course of annealing of metal-oxide composites in air at 500 °C, palladium nanoparticles must be oxidized to PdO. The fact that surface layers contain Pd^0 in addition to Pd^{2+} can be explained by presence of siloxane-acrylate emulsion decomposition products which are served as reducing agents. Taking into account the XPS data, the Pd-containing composites can be represented as $PdO_x/SiO_2 + TiO_2/Ti$, where $0 < x \leq 1$.

On the other hand, according to the energy-dispersive analysis (analysis depth ~1 μm), the increase of the number of dipping-drying operations with subsequent annealing results in changes in the volume-average composite element composition (Fig. 4). The gradual decrease of the silicon and oxygen concentrations and the increase of the titanium content take place. Also, the palladium concentration increases (from 0.04 at.% at N = 5–0.16 at.% at N = 20).

The coatings morphology changes along with the number of depositions N (Fig. 5). The surface of initial PEO-coatings comprises a complex structure consisting of individual protruding spherical elements and fused particles of different shapes, most of which are randomly positioned on the surface and alternate with pores and

Table 1
Element composition of surface layers of a thickness of about 3 nm for Pd-containing composites, form XPS data.

Sample	C, at %							
	Na 1s	O 1s	Ti $2p_{1/2}$	Pd $3d_{5/2}$	C 1s	Si 2p	Na_{Auer}	N
5Pd	0.9/0.8	59.2/63.0	6.0/7.4	0.1/0.3	18.0/11.4	15.3/17.1	0.6/0.4	
10Pd	0.3/0.8	58.9/61.4	6.2/8.4	0.1/0.3	16.5/9.6	17.4/18.7	0.1/0.1	0.5/0.9
20Pd	–	57.8/62.1	5.4/6.9	0.1/0.2	18.3/10.1	17.3/19.8	0.1/0.1	1.1/0.8

Note: numerator – element composition of sample surface layers, denominator – the same for subsurface layers (upon argon etching, E_{kin} = 5000 eV, t = 5 min).

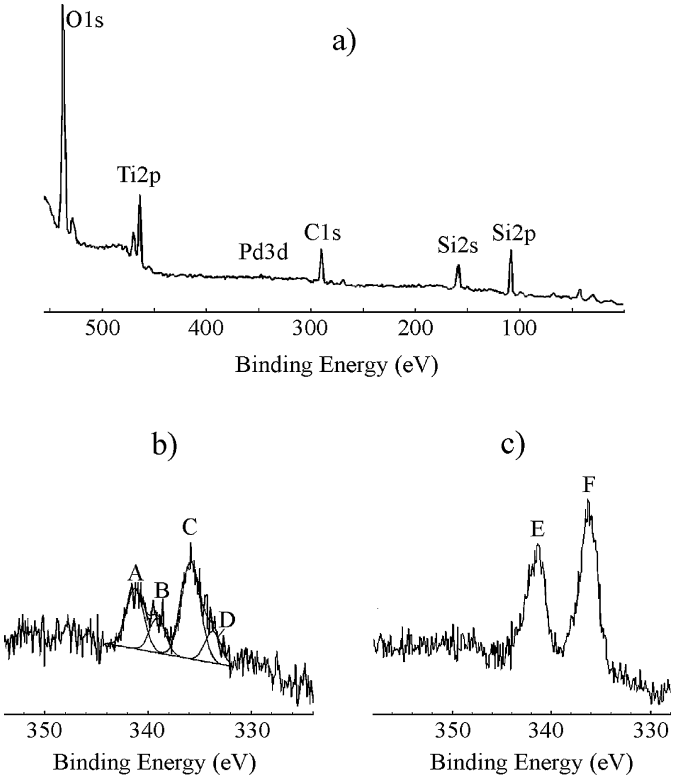

Fig. 3. XPS spectra of the sample 10 Pd: overall spectrum (a), Pd 3d spectrum before (b) and (c) after etching with argon ions.
A, C – Pd^{2+} (342.3, 336.9 eV)
B, D – Pd^{0} (340.1, 335.0 eV)
E, F – Pd^{+} (341.4, 336.1 eV).

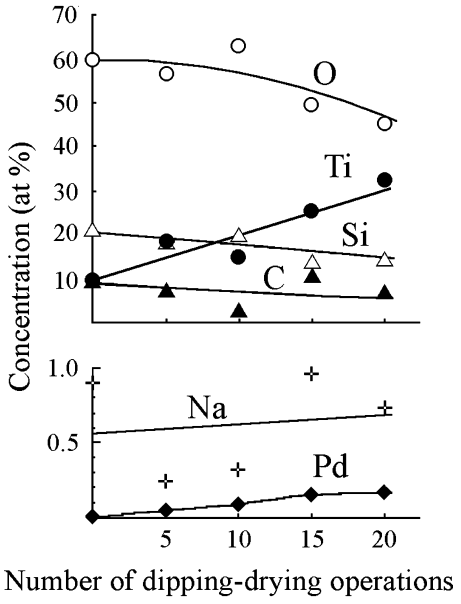

Fig. 4. Effect of the number of dipping-drying operations N on the element composition of the sample surface, according to the energy-dispersive analysis data.

cavities (Fig. 5a). At 5-fold deposition with subsequent annealing, one observes new objects on the surface – elongated thread-like formations ("bundles" or "bridges", see I in Fig. 5b). Along with the N increase, thread-like elements are transformed into parts occupying larger areas of the initial coatings ("smooth" sites I in Fig. 5c–e). The sites are coated with a network of cracks. According to SEM images (Fig. 5d), the thickness of these sites is 1–3 μm. At $N \geq 15$, there appear, along with elevated sites I on the surface of formed composite layers, the sites with absent initial II and deposited coating layers ("glades" III in Fig. 5f).

Table 2 shows the composition of some parts of the composite coating formed with N = 20 and annealed determined using an energy-dispersive accessory. The palladium distribution over individual surface parts at different N is shown in a diagram (Fig. 6). As seen from the obtained data, palladium concentrates in sites I deposited from sol. "Glades" are essentially parts of uncoated titanium. In the composition of the initial coating (sites II, compare with Fig. 4, N = 0) upon annealing, the titanium concentration grows, while the carbon content decreases.

Since palladium concentrates in smooth bulk (of a thickness of about 1–3 μm) sites emerged as a result of annealing of titanium hydroxide gel containing nanoparticles of palladium, which was formed at drying of the deposited sol, the structure and composition of these very sites were studied in more detail. The surface of smooth sites is nanostructured and built of particles of a size of ~3–11 nm, see Fig. 7c. Spherical morphological objects of a size of ~25–60 nm (see Fig. 7a, b) are rather homogeneously distributed over the sites surface and bulk. The presence of such objects in the bulk is indicated by different degrees of their manifestation on the images. As follows from the element analysis data obtained for sites 1 and 2 in Fig. 7c, palladium concentrates in spherical objects of a size of ~25–60 nm.

The results of catalytic tests of the samples in the reaction of oxidation of CO into CO_2 are shown in Fig. 8 and Table 3. A noticeable conversion of CO into CO_2 is observed at temperatures above 170 °C. Analysis of the data presented in Fig. 8 and Table 3 demonstrates

Table 2
Element composition of surface structures for the sample 20Pd.

Element	Types of composite layers sites		
	Sites of initial coating after annealing	Deposited layers	Areas without coating
	"Rough" sites (II)	"Smooth" sites (I)	"Glades" (III)
C	4.86	7.5	1.78
O	55.38	51.75	19.28
Na	0.36	1.26	0.11
Si	17.76	23.27	0.97
Ti	21.61	15.8	77.83
Pd	0.03	0.42	0.03
Total	100	100	100

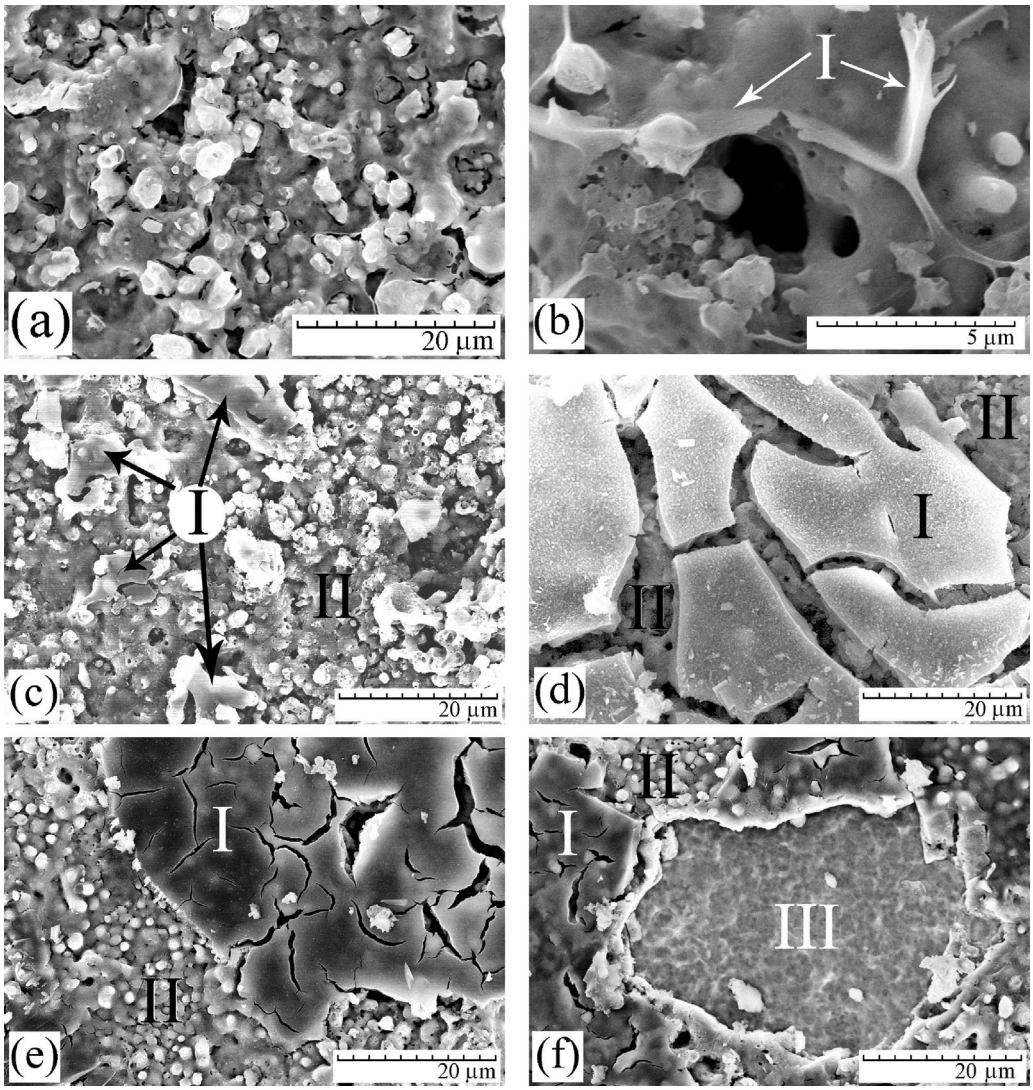

Fig. 5. SEM images of the surface of samples $SiO_2 + TiO_2$/Ti (a), 5Pd (b), 10Pd (c), 15Pd (d) and 20Pd (e, f). Markings: I – deposited sites, II – initial coating upon annealing, III – site without coating.

that the reaction rate W_{50} at the same temperatures is virtually identical for the samples 10Pd, 15Pd, and 20Pd and significantly lower for the samples 5Pd. The catalytic activity in CO oxidation is manifested by initial PEO-coatings as well, but at much higher temperatures (above 300 °C). In the reaction on Pd-containing composites in the temperature range 200–320 °C one can mark out two stages of the catalytic process (stages K, D, Fig. 8). The calculated activation energy for the stage K (at temperatures 200–270 °C) is 46–55 kJ/mol characteristic for the kinetic stage [58]. At temperatures above 270 °C, there occurs the transfer from the kinetic to the diffusion (D) stage of CO oxidation.

It should be noted when calculating the reaction rate we used the weight of the sample (wire + coating) because the mass of palladium is difficult to calculate. The estimates suggest that upon 10-fold deposition of sol the weight of palladium applied is $\sim 3 \times 10^{-8}$ g (geometric area of the sample is 20 cm^2, the concentration of palladium in sol is 0.08 mg/mL, the area occupied by the sol on the surface of the sample in Fig. 4c is ~20%; the thickness of the applied layer ~1 μm). Upon 5-fold deposition it may be about $\sim 1 \times 10^{-8}$ g. If the reaction rate is normalized by the weight of palladium instead of the sample weight the slope and the activation energy will not change but the comparative ratio

Table 3
Reaction rate W_{50} and activation energy E_a for CO oxidation* in the temperature range ΔT for samples with different palladium concentrations.

Sample	C_{Pd}, at.%	$W_{50} \times 10^3$, mL/g s					ΔT, °C	E_a, kJ/mol
		200 °C	250 °C	300 °C	320 °C	350 °C		
$SiO_2 + TiO_2$/Ti	0	–	–	–	0.35	0.52	320–420	42.55
5Pd	0.04	1.15	5.47	9.84	10.65	–	200–270	54.48
10Pd	0.09	4.25	20.55	29.72	28.15	–	200–270	46.20
15Pd	0.15	6.75	20.07	23.26	20.81	–		
20Pd	0.16	6.80	20.46	23.14	26.97	–		

* $m_{cat.} \approx 2.5$ g (titanium wire + PEO coating + deposited layer), $S_{geom.} = 20$ cm^2, $C_{CO} = 1$ vol.% in air.

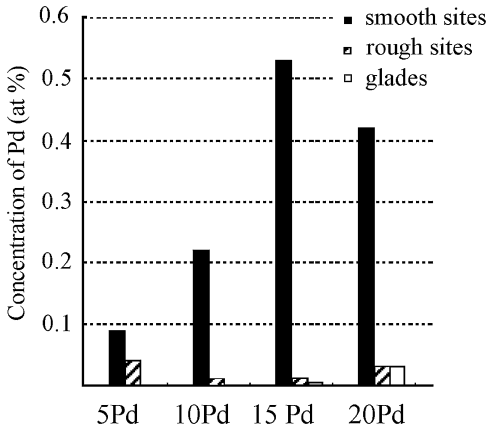

Fig. 6. Diagram of palladium distribution in the compositions of sample surface structures.

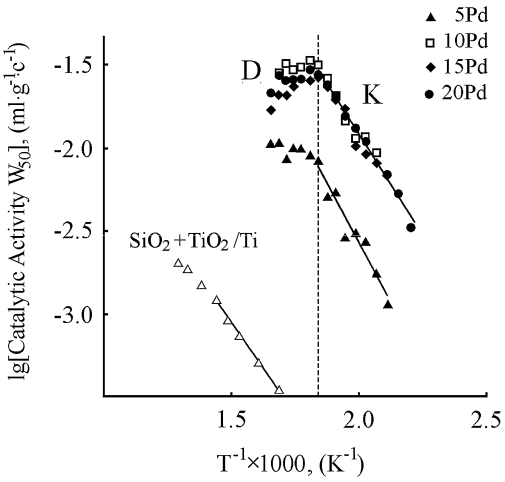

Fig. 8. Dependencies of the logarithm of catalytic activity W_{50} (mL/g s) on the inverse temperature ($T^{-1} \times 1000$, K^{-1}) for composites $SiO_2 + TiO_2$/Ti and samples 5Pd, 10Pd, 15Pd, and 20Pd with different palladium content (Table 3). The CO oxidation reaction rate is calculated for $X = 50\%$. The dashed line divides the kinetic (K) and diffusion (D) areas of the reaction of CO oxidation over Pd-containing samples. Reaction conditions: $m_{cat.} \approx 2.5$ g (titanium wire + PEO coating + deposited layer), $S_{geom.} = 20$ cm^2, $C_{CO} = 1$ vol.% in air.

between curves will change. Curve of 5Pd in Fig. 8 will probably shift upper.

4. Discussion

To sum up, combination of the methods of plasma electrolytic oxidation and template sol–gel synthesis enables one to fabricate metal-oxide composites with palladium nanoparticles attached and distributed over the surface, see Fig. 1. Such composites are active in oxidation of CO into CO_2 at temperatures above 170 °C.

The obtained data allow assuming the following sequence of processes occurring during the formation of such composites. At the first dipping, sol partially wets the surface mostly on sites of the initial PEO-coatings adjacent to pores (Fig. 5b). Upon drying (at 90 °C) sol is transformed into gel. Subsequent dipping-drying operations yield the addition of new portions to the gel attached to the surface. At 5-fold repetition of the dipping-drying operations ($N = 5$), the gel remained on the surface and undergone annealing at 500 °C condenses into elongated thread-like structures (Fig. 5b). When N increases, the amount of gel attached to the surface increases as well. New portions of gel must concentrate around the already formed parts, since no new thread-like structures were observed in the course of N increase. Attachment of new portions of gel as a result of annealing yields the formation of parts occupying some specific surface area, i.e., a gradual transformation of thread-like structures into flat ones (Fig. 5c). Along with the N increase, the area of such sites increases as well (Fig. 5d, e). Here, sites of the new phase (I) formed at annealing undergo cracking. The latter can

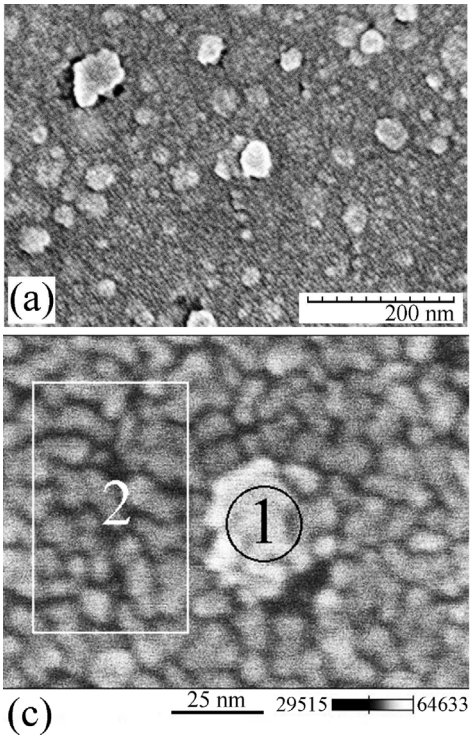

Element	C, at %	
	1	2
C	22.93	19.58
O	32.23	32.04
Na	-	0.93
Si	26.19	27.54
Ti	18.38	19.90
Pd	0.26	0.01
Σ	99.99	100.00

Fig. 7. SEM images of the surfaces of smooth sites (a, b) and composition of the analyzed sites (c) for the sample 20Pd.

be caused by a number of factors, including dehydration and gel compression on less compressible substrate upon heating.

Along with the increase of the dipping-drying operations number ($N \geq 15$), sites of uncoated titanium ("glades", Fig. 5f, Table 2) emerge on the coating surface. Their formation is probably caused by the etching effect of sol containing chloride ions in the acidic medium.

According to the obtained data, in the process of drying the used sol containing titanium hydroxide and micelles of siloxane-acrylate emulsion with immobilized palladium nanoparticles transforms into gel, whose annealing results in the formation of a porous material containing predominantly TiO_2 in the anatase modification, whereas palladium is fixed in pores formed due to destruction of emulsion micelles [57]. In our case, the layer deposited using the template sol–gel synthesis contains significant amounts of not only titanium, but also of carbon and silicon, see Fig. 7. It is evident that carbon and silicon are the products of emulsion thermal destruction. Since the oxygen concentration is insufficient for formation of stoichiometric oxides (TiO_2, SiO_2), the above elements must exist in lower oxidation states. This conclusion is indirectly corroborated by the XPS data on the presence, along with Ti^{4+}, of titanium in lower oxidation states in coatings.

Palladium concentrates in the deposited layers and is included in nanoparticles (25–60 nm) that are rather homogeneously distributed over the surface and bulk of the deposited layer, see Fig. 7. The energy-dispersive analysis registers, aside from palladium, the products of emulsion and gel destruction in the composition of such particles. Possibly, these particles are hollow, i.e., comprise pores formed as a result of burning out of siloxane-acrylate emulsion micelles, just like at fabrication of bulk porous materials [30,31,57]. The presence of carbon, oxygen, silicon, and titanium in them must be related to high penetrating ability of the focused electron beam (down to ~1 μm) during the energy-dispersive analysis and the contribution of lower layers containing gel destruction products.

The dimensions of Pd particles produced by other methods are from 1 nm to tens and hundreds microns [16,26], which are comparable to that obtained in the present work (25–60 nm). Thus using the combination of PEO and template sol–gel synthesis allows one to obtain Pd-based catalysts with good noble metal dispersion. Additionally the resulting catalysts have the advantage of a metal substrate providing high thermal conductivity.

According to the XPS data, independently of the number of dipping-drying operations *N*, the composition of surface and subsurface layers averaged over the area (to a depth of down to ~6 nm) remains virtually the same $N \geq 5$, see Table 1. The latter must be determined by the ratio of areas of Pd-containing deposited layers and formed at $N \geq 15$ sites of uncoated titanium ("glades") and by the presence of some specific fraction of palladium over the whole surface.

The data of catalytic tests (Fig. 8) and element analysis on the palladium content in deposited layers (Fig. 6) show that 10-fold deposition of the applied sol on silicate PEO-coatings on titanium is sufficient to fabricate quality Pd-containing coatings active in oxidation of CO into CO_2. Using a greater amount of expensive Pd does not result in sufficient improving the catalytic performance. The composites fabricated at $N = 10$ are mechanically stable and do not crumble during manipulations with them. One should mention that the initial PEO-coatings ($SiO_2 + TiO_2$) on titanium are characterized by some catalytic activity (Fig. 8). However, the CO oxidation rate over them is 2.07×10^{-3} mol/L even at 500 °C, i.e., it just approaches the reaction rate on Pd-containing composites at 200 °C.

The fact that upon further *N* increase the catalytic activity of composites does not grow can be explained as follows. Along with the increase of the dipping number, the palladium concentration in the deposited layers composition increases, but, at the same time, the emerge "glades" with almost no palladium (Figs. 5 and 6). As a result, the area of Pd-containing parts increases insignificantly. Active centers on the surface are responsible for composites catalytic properties. As shown by the data from Table 1, the palladium concentration on the surface does not increase. Therefore, the composite activity increase observed upon transition from $N = 5$ к $N = 10$ is not present anymore. Thus, it is the experimentally determined that when Pd-containing catalysts are fabricated by combining PEO and template sol–gel synthesis, the dipping-drying operations number can be optimized in order to reduce consumption of the expensive palladium.

Catalytic properties of Pd-containing catalysts are known [29] to depend significantly on the support nature. For instance, depending on the support nature, the temperature corresponding to 50% conversion of CO (T_{50}) increases in the row: CeO_2 (45 °C) < ZrO_2 (165 °C) < TiO_2 (185 °C) < Al_2O_3 (205 °C) < SiO_2 (255 °C) [29]. In our case ($SiO_2 + TiO_2$), 50% is observed at $T_{50} \geq 180$°C (at flow rate ~50 mL/min). Possibly, in the course of dipping, sol is predominantly sorbed on the coating sites containing titanium oxide.

The composition, structure, porosity, roughness and other parameters of PEO-coatings depend on the nature of treated metal, electrolyte composition and temperature, and formation electric and timing parameters [13,29,52,53,59]. In particular, the PEO method allows fabricating on valve metals oxide layers containing γ- and α-Al_2O_3, TiO_2, SiO_2, ZrO_2, CeO_x, VO_x, WO_3, MoO_3 or their mixtures [60–72] and embed noble metals into the layers [42–45,73–75]. It is possible that at using PEO-coatings of different compositions as supports the combination of methods would enable one to fabricate active catalysts for heterogeneous processes.

In the present work, we used sol of titanium hydroxide containing micelles of siloxane-acrylate emulsion with immobilized palladium nanoparticles as a template. As was shown here, PEO-coatings are deposited with a layer containing, aside from palladium nanoparticles, TiO_2 and products of emulsion destruction. Application of sols and templates of different natures could promote fabrication of catalytically active structures on metallic substrates. For instance, deposition of sols based on hydroxides of manganese, tungsten, cobalt, nickel, iron and other transition metals forming catalytically active oxides upon annealing could allow formation of composite promising for application in catalysis: M^1/M^2O_y/PEO-coating/M^3, where M^1 – noble metal, M^2 – transition metal, M^3 – valve metal (Al, Ti, Mg, Zr etc.). One should mention that coatings containing, along with noble metals, cobalt, nickel, or iron oxides could be characterized not only by catalytic activity, but also by ferromagnetic properties. The latter was demonstrated for coatings on titanium containing copper and iron oxides [76]. In our opinion, application of the combination of methods opens new prospects in formation of functional composites of the 'coating/metal' type.

5. Conclusions

In has been demonstrated that application of the combination of methods of plasma electrolytic oxidation and template sol–gel synthesis enables one to form composites $PdO_x/SiO_2 + TiO_2$/Ti containing palladium nanoparticles attached and distributed over the surface. The resulting catalysts with disperse particles of a size of 25–60 nm have the advantage of the metal substrate, which provides high thermal conductivity. The average palladium concentration on the composite surface depends on the multiplicity of sol deposition and attains 0.2 at.% Pd. In such systems, palladium is present in forms Pd^0 and PdO. The formed composites are active in oxidation of CO into CO_2 at temperatures above 170 °C. The data of catalytic tests and element analysis on the palladium content in deposited layers show that 10-fold deposition of the applied sol on

silicate PEO-coatings on titanium is sufficient to fabricate quality Pd-containing coatings active in oxidation of CO into CO_2, which allows one to optimize consumption of the expensive palladium. Application of the combination of methods of plasma electrolytic oxidation and template sol–gel synthesis is promising in fabrication of layers of various composition and purpose on metallic substrates.

Acknowledgments

The work was partially supported by grants nos. 12-III-A-04-048 and 13-III-B-04-043 of the Presidium of the Far Eastern Branch, Russian Academy of Sciences.

References

[1] J. Kaspar, P. Fornasiero, N. Hickey, Catal. Today 77 (4) (2003) 419–449.
[2] A.V. Krylova, A.I. Mikhailichenko, Khim. Tekhnol. (2) (2003) 13–21 (in Russian).
[3] N.M. Popova, Vehicle Exhaust Catalysts, Nauka, Almaty, 1987 (in Russian).
[4] G. Centi, J. Mol. Catal. A: Chem. 173 (1–2) (2001) 287–312.
[5] M.V. Twigg, Catal. Today 163 (1) (2011) 33–41.
[6] P. Avila, M. Montes, E.E. Miro, Chem. Eng. J. 109 (1–3) (2005) 11–36.
[7] N.M. Popova, G.A. Savel'eva, Theor. Exp. Chem. 27 (6) (1991) 560–566.
[8] I.A. Kurzina, F.J.C.S. Aires, G.G. Cervantes, J.C. Bertolini, Russ. J. Phys. Chem. 80 (10) (2006) 1661–1665.
[9] A. Satsuma, K. Osaki, M. Yanagihara, J. Ohyama, K. Shimizu, Appl. Catal. B-Environ. 132 (2013) 511–518.
[10] N. Imanaka, T. Masui, K. Yasuda, Chem. Lett. 40 (8) (2011) 780–785.
[11] P.A. Carlsson, M. Skoglundh, Appl. Catal. B-Environ. 101 (3–4) (2011) 669–675.
[12] O.V. Mokhnachuk, S.A. Solov'ev, A.I. Senkevich, Theor. Exp. Chem. 42 (1) (2006) 48–52.
[13] S. Specchia, G. Toniato, Catal. Today 147 (2009) S99–S106.
[14] T. Dangsawai, P. Praserthdam, J.B. Kim, T. Inui, Adv. Environ. Res. 3 (2000) 450–458.
[15] N. Li, Q.Y. Chen, L.F. Luo, W.X. Huang, M.F. Luo, G.S. Hu, J.Q. Lu, Appl. Catal. B-Environ. 142–143 (2013) 523–532.
[16] X.-Z. Jiang, S.-J. Yang, S.-H. Wu, Platinum Met. Rev. 37 (2) (1993) 72–75.
[17] V.S. Narkhede, A. De Toni, V.V. Narkhede, M. Guraya, J.W. Niemantsverdriet, M.W.E. van den Berg, W. Grunert, H. Gies, Microporous Mesoporous Mater. 118 (1–3) (2009) 52–60.
[18] M. Haruta, Gold Bull. 37 (1) (2004) 27–36.
[19] D.W. Wyrwa, G. Schmid, J. Clust. Sci. 18 (3) (2007) 476–493.
[20] S. Bonanni, K. Ait-Mansour, H. Brune, W. Harbich, ASC Catal. 1 (4) (2011) 385–389.
[21] P.W. Seo, H.J. Choi, S.I. Hong, S.C. Hong, J. Hazard. Mater. 178 (1–3) (2010) 917–925.
[22] A. de Lucas-Consuegra, F. Dorado, J.L. Valverde, R. Karoum, P. Vernoux, Catal. Commun. 9 (1) (2008) 17–20.
[23] M. Haruta, N. Yamada, T. Kaboyashi, S. Iijima, J. Catal. 115 (1989) 301–309.
[24] G.C. Bond, D.T. Thompson, Gold Bull. 33 (2000) 41–51.
[25] A.S. Lisitsyn, V.N. Parmon, V.K. Duplyakin, V.A. Likholobov, Ros. Khim. Zhurn. 50 (4) (2006) 140–153 (in Russian).
[26] M.L. Toebes, J.A. van Dillen, K.P. de Jong, J. Mol. Catal. A – Chem. 173 (1–2) (2001) 75–98.
[27] T. Uematsu, L. Fan, T. Maruyama, N. Ichikuni, S. Shimazu, J. Mol. Catal. A – Chem. 182 (1) (2002) 209–214.
[28] Y. Hatakeyama, K. Onishi, K. Nishikawa, RSC Adv. 1 (9) (2011) 1815–1821.
[29] M.-F. Luo, Z.-Y. Hou, X.-X. Yuan, X.-M. Zheng, Catal. Lett. 50 (3–4) (1998) 205–209.
[30] V.A. Avramenko, S.Yu. Bratskaya, P.A. Karpov, V.Yu. Mayorov, A.Yu. Mironenko, M.S. Palamarchuk, V.I. Sergienko, Dokl. Phys. Chem. 435 (2010) 193–197, Part 2.
[31] E.K. Papynov, V.Yu. Mayorov, M.S. Palamarchuk, S.Yu. Bratskaya, V.A. Avramenko, J. Sol-Gel. Sci. Technol. 68 (3) (2013) 374–386.
[32] P.T. Patil, A. Dimitrov, H. Kirmse, W. Neumann, E. Kemnitz, Appl. Catal. B-Environ. 78 (1–2) (2008) 80–91.
[33] X.K. Wang, X.Y. Tan, Z.X. Zhang, C.Y. Bao, C.T. Williams, C.H. Liang, Micro Nano Lett. 7 (9) (2012) 901–903.
[34] N. Sahu, K.M. Parida, A.K. Tripathi, V.S. Kamble, Appl. Catal. A-Gen. 399 (1–2) (2011) 110–116.
[35] Y.Y. Zhang, M.C. Zhang, X. Zhang, X.H. Wang, W.Q. Zhang, Chem. Eng. J. 215 (2013) 96–104.
[36] S.F. Tikhov, G.V. Chernykh, V.A. Sadykov, A.N. Salanov, G.M. Alikina, S.V. Tsybulya, V.F. Lysov, Catal. Today 53 (4) (1999) 639–646.
[37] F. Patcas, W. Krysmann, Appl. Catal. A-Gen. 316 (2) (2007) 240–249.
[38] W. Ehrfeld, V. Hessel, H. Löwe, Microreactors: New Technology for Modern Chemistry, Wiley-VCH, Weinheim, 2000.
[39] G. Kolb, H. Pennemann, R. Zapf, Catal. Today 110 (1–2) (2005) 121–131.
[40] T. Baier, G. Kolb, Chem. Eng. Sci. 62 (17) (2007) 4602–4611.
[41] J.R.H. Carucci, K. Arve, K. Eranen, D.Y. Murzin, T. Salmi, Catal. Today 133 (2008) 448–454.
[42] L.M. Tyrina, V.S. Rudnev, A.Yu. Ustinov, I.V. Lukijyanchuk, P.M. Nedozorov, Inorg. Mater. 45 (4) (2009) 414–417.
[43] L.M. Tyrina, V.S. Rudnev, T.P. Yarovaya, A.Yu. Ustinov, I.V. Lukiyanchuk, V.V. Permyakov, Russ. J. Appl. Chem. 83 (4) (2010) 680–686.
[44] L.M. Tyrina, V.S. Rudnev, P.M. Nedozorov, A.Yu. Ustiniov, I.V. Lukiyanchuk, T.A. Kaidalova, Russ. J. Inorg. Chem. 56 (9) (2011) 1429–1435.
[45] V.S. Rudnev, L.M. Tyrina, I.V. Lukiyanchuk, T.P. Yarovaya, I.V. Malyshev, A.Yu. Ustinov, P.M. Nedozorov, T.A. Kaidalova, Surf. Coat. Technol. 206 (2–3) (2011) 417–424.
[46] N.V. Lebukhova, V.S. Rudnev, P.G. Chigrin, I.V. Lukiyanchuk, M.A. Pugachevsky, A.Yu. Ustinov, E.A. Kirichenko, T.P. Yarovaya, Surf. Coat. Technol. 231 (2013) 144–148.
[47] V.S. Rudnev, M.S. Vasilyeva, N.B. Kondrikov, L.M. Tyrina, Appl. Surf. Sci. 25 (5) (2005) 1211–1220.
[48] V.S. Rudnev, L.M. Tyrina, A.Yu. Ustinov, S. Vybornova, I.V. Lukiyanchuk, Kinet. Catal. 51 (2) (2010) 266–272.
[49] M.S. Vasilyeva, V.S. Rudnev, A.Yu. Ustinov, I.A. Korotenko, E.B. Modin, O.V. Voitenko, Appl. Surf. Sci. 257 (4) (2010) 1239–1246.
[50] M.S. Vasilyeva, V.S. Rudnev, F. Wiedenmann, S. Wybornov, T.P. Yarovaya, X. Jiang, Appl. Surf. Sci. 258 (2) (2011) 719–726.
[51] M.S. Vasil'eva, V.S. Rudnev, O.E. Sklyarenko, L.M. Tyrina, N.B. Kondrikov, Russ. J. Gen. Chem. 80 (8) (2010) 1557–1562.
[52] V.S. Rudnev, Prot. Met. 44 (3) (2008) 263–272.
[53] F.C. Walsh, C.T.J. Low, R.J.K. Wood, K.T. Stevens, J. Archer, A.R. Poeton, A. Ryder, Trans. Inst. Met. Finish. 87 (3) (2009) 122–135.
[54] A.L. Yerokhin, X. Nie, A. Leyland, A. Matthews, S.J. Dowey, Surf. Coat. Technol. 122 (2–3) (1999) 73–93.
[55] B.L. Jiang, Y.M. Wang, in: H. Dong (Ed.), Surface Engineering of Light Alloys, Woodhead Publishing Limited, Oxford–Cambridge–New Delhi, 2010, pp. 110–154.
[56] S.Yu. Grilikhes, Metal Degreasing, Etching and Polishing, Mashinostroenie, Leningrad, 1977 (in Russian).
[57] H.H. Wang, X.R. Li, G.Q. Fei, J. Mou, Express Polym. Lett. 4 (11) (2010) 670–680.
[58] G.M. Panchenkov, V.P. Lebedev, Chemical Kinetics and Catalysis, Mir Publishers, Khimiya, Moscow, 1976.
[59] J.A. Curran, T.W. Clyne, Acta Mater. 54 (7) (2006) 1985–1993.
[60] P.S. Gordienko, V.S. Rudnev, S.V. Gnedenkov, T.P. Yarovaya, O.A. Khrisanfova, V.I. Tyrin, L.M. Tyrina, Russ. J. Appl. Chem. 68 (6) (1995) 854–857.
[61] G.A. Markov, A.I. Slonova, O.P. Terleeva, Prot. Met. 33 (3) (1997) 257–262.
[62] J.A. Liu, X.Y. Zhu, Z.Q. Huang, S.R. Yu, X.Z. Yang, J. Coat. Technol. Res. 9 (3) (2012) 357–363.
[63] Z.P. Yao, Z.H. Jiang, X.L. Zhang, J. Am. Ceram. Soc. 89 (9) (2006) 2929–2932.
[64] E. Matykina, R. Arrabal, F. Monfort, P. Skeldon, G.E. Thompson, Appl. Surf. Sci. 255 (5) (2008) 2830–2839.
[65] Z.P. Yao, Y.L. Jiang, Z.H. Jiang, F.P. Wang, Z.D. Wu, J. Mater. Process. Technol. 205 (1–3) (2008) 303–307.
[66] Z.D. Wu, Z.P. Yao, Z.H. Jiang, Rare Metals 27 (1) (2008) 55–58.
[67] M.R. Bayati, A.Z. Moshfegh, F. Golestani-Fard, Appl. Surf. Sci. 256 (9) (2010) 2903–2909.
[68] J. He, Q. Luo, Q.Z. Cai, X.W. Li, D.Q. Zhang, Mater. Chem. Phys. 129 (1–2) (2011) 242–248.
[69] V.V. Shtefan, A.Y. Smirnova, Rus. J. Appl. Chem. 86 (12) (2013) 1842–1846.
[70] V.S. Rudnev, T.P. Yarovaya, P.M. Nedozorov, A.Yu. Ustinov, L.M. Tyrina, I.V. Malyshev, V.G. Kuryavyi, V.S. Egorkin, S.L. Sinebryukhov, S.V. Gnedenkov, Prot. Met. Phys. Chem. Surf. 47 (5) (2011) 621–628.
[71] V.S. Rudnev, I.V. Lukiyanchuk, V.V. Kon'shin, P.S. Gordienko, Russ. J. Appl. Chem. 75 (7) (2002) 1082–1086.
[72] P.S. Gordienko, V.S. Rudnev, T.I. Orlova, A.G. Kurnosova, A.G. Zavidnaya, A.S. Rudnev, V.I. Tyrina, Prot. Met. 29 (5) (1993) 602–605.
[73] H.S. Ryu, S.H. Hong, Electrochem. Soc. 157 (4) (2010) C131–C136.
[74] W.H. Song, H.S. Ryu, S.H. Hong, J. Biomed. Mater. Res. A 88A (1) (2009) 246–254.
[75] N. Salami, M.R. Bayati, F. Golestani-Fard, H.R. Zargar, Mater. Res. Bull. 47 (4) (2012) 1080–1088.
[76] I.V. Lukiyanchuk, V.S. Rudnev, A.Yu. Ustinov, V.P. Morozova, M.V. Adigamova, L.M. Tyrina, I.V. Chernykh, Russ. J. Appl. Chem. 85 (11) (2012) 1686–1690.